energy&fuels

pubs.acs.org/EF

Article

Prospects of the Novel CSAR Concept for Fully Electric or Flexible Electric−Thermal Hybrid CO_2 Capture from CHP Plants

Schalk Cloete, Chaitanya Dhoke, Davide Bonalumi, John Morud, Antonio Giuffrida, Matteo Carmelo Romano, and Abdelghafour Zaabout*

Cite This: *Energy Fuels* 2023, 37, 12030−12044

Read Online

ACCESS | Metrics & More | Article Recommendations | Supporting Information

ABSTRACT: Momentum is gathering behind the goal of achieving net-zero CO_2 emissions by 2050 in Europe and around the world. Negative emissions via biomass or waste combustion with CO_2 capture can make net zero considerably easier to achieve. This study investigates CO_2 capture from combined heat and power (CHP) plants that often use bio-based fuels. However, most CO_2 capture processes require large amounts of heat, potentially consuming most of the CHP plant's primary product. The novel continuous swing adsorption reactor (CSAR) concept provides a promising solution by capturing CO_2 using electrically driven heat and vacuum pumps. Techno-economic assessments conducted in this work illustrate that CSAR clearly outperforms an MEA benchmark when the CHP plant sells heat throughout the year (MEA would need a heat price below 10 €/MWh at an electricity price of 60 €/MWh to compete). When large amounts of free heat are available in summer months, MEA becomes more attractive, but a flexible CSAR configuration utilizing free heat during summer maintains a clear advantage for CSAR (MEA needs a heat price below 15 €/MWh at an electricity price of 60 €/MWh). Stronger competition arises from advanced solvents such as PZ/AMP that can match CSAR at almost double the heat price of MEA. Still, CSAR will remain attractive in most cases, especially for retrofits where considerable capital expenditures would be required to provide existing heat customers with an alternative heat supply if solvent technologies are used. Thus, CSAR appears to be a promising technology for achieving negative emissions from CHP plants.

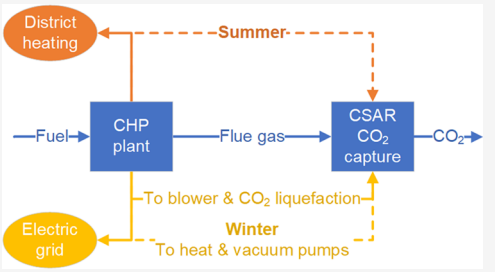

1. INTRODUCTION

CO_2 capture and storage (CCS) can play a prominent role in reducing global CO_2 emissions. The application of CCS to fossil fuel energy infrastructure can avoid most of the greenhouse gases that would otherwise accumulate in the atmosphere. Furthermore, CCS can enable net greenhouse gas removal if the captured CO_2 originates from biomass or directly from the atmosphere. The potential negative emission enabled by CCS is a key reason why the IPCC found that achieving decarbonization pathways consistent with the Paris Agreement[1] will be more than twice as costly (and possibly not even practically achievable) without CCS.[2] The recent IEA special report on CCS agrees that reaching net-zero emissions without CCS will be virtually impossible.[3] Most of the scenarios in the IPCC report on 1.5° of global warming also rely on large amounts of negative emissions.[4] Scenarios without negative emissions tend to require substantial reductions in global energy demand that are not realistic in a world where almost 5 billion people still live on less than 10 $/day.[5]

CCS from biomass combustion (BECCS) is generally viewed as the most economical pathway to large-scale CO_2 removal and is relied upon heavily in the aforementioned assessments. However, biomass production has large land-use impacts that can strongly reduce its CO_2 avoidance and increase its overall environmental impact. Depending on the assumptions regarding direct and indirect land-use changes associated with BECCS, life cycle CO_2 emissions could even remain positive after 50 years of operation. A sensitivity analysis by Fajardy and Dowell[6] indicates a range of CO_2 emissions of −1000 to 200 ton/ha over a 50-year operating life, depending on various assumptions when miscanthus is used. Woody biomass from willow performs worse, returning mostly positive lifecycle emissions.

An alternative is waste-to-energy (WTE) where lifecycle emissions can be low or even slightly negative before any CCS is applied due to the CO_2 avoided by energy recovery from this fuel that would otherwise end up in landfills (which is associated with CH_4 emissions) or be incinerated without energy recovery.[7] Here, a distinction should be drawn between negative life cycle emissions and CO_2 removal: WTE can achieve negative emissions by avoiding emissions from alternative fossil-based energy supply and methane from landfills that would otherwise occur, but it cannot remove CO_2 from the atmosphere. However, the addition of CCS to WTE plants can unlock not

Received: March 21, 2023
Revised: July 8, 2023
Published: August 7, 2023

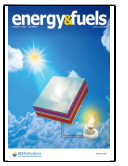

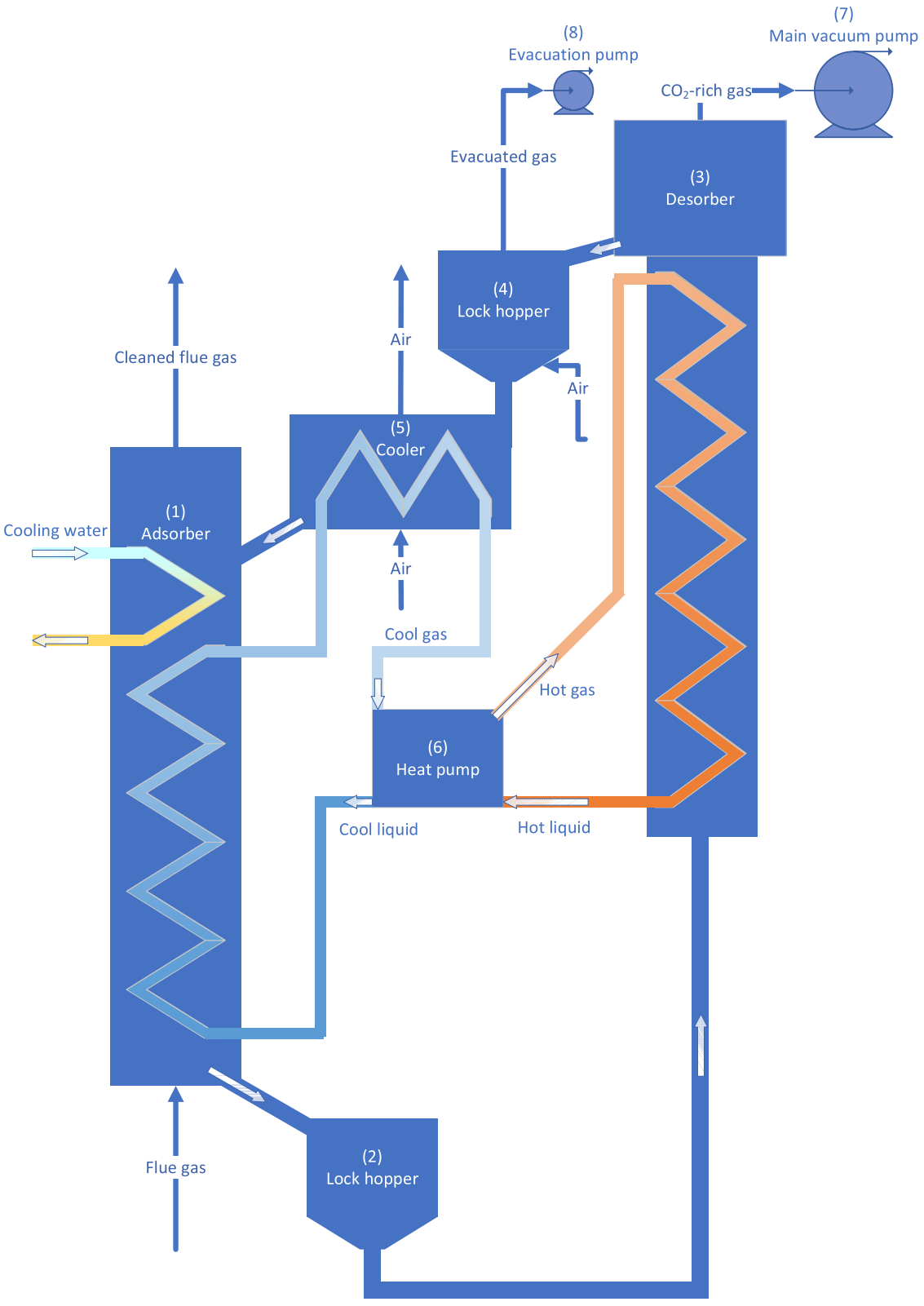

Figure 1. Illustration of the CSAR working principle.

only negative life cycle emissions but also net CO_2 removal if the CO_2 capture ratio and the biogenic fraction in the waste are sufficiently high.

From an economic viewpoint, applying CCS to WTE plants that produce only electricity has a severe negative effect on levelized costs. Due to the challenging nature of the fuel, these plants typically operate at low efficiencies, producing large amounts of CO_2 per unit of electricity produced. Capturing and compressing all this CO_2 consumes more than half of the power output, causing high costs.[8,9] More efficient CO_2 capture can lower these high costs, prompting investigations involving various advanced CO_2 capture technologies, including moving

https://doi.org/10.1021/acs.energyfuels.3c00885
Energy Fuels 2023, 37, 12030−12044

bed temperature swing adsorption,[10] calcium looping,[11] and vacuum swing adsorption.[12]

For CHP plants that extract a much larger amount of useful energy from the fuel, adding CCS can be considerably cheaper. For example, addition of CCS becomes feasible at a CO_2 tax around 30−40 €/ton in a combined heating, cooling, and power plant with biomass co-firing.[13] However, such attractive costs require very-low-grade heat to be usable for district heating so that heat from exothermic CO_2 capture reactions and flue gas condensers can be productively used (in this case,[13] heated water is assumed to leave the plant at 94 °C and return at 43 °C). Another study shows 63 €/ton in CO_2 avoidance costs when the CHP plant is integrated with a geothermal heat source.[14] There is also a potentially large addressable market for CHP plants in providing heat for CO_2 capture retrofits. This strategy can be cheaper than direct CO_2 capture from coal plants with a CO_2 tax requirement of 55 $/ton (~50 €/ton).[15] Industrial CHP offers another interesting application, where the addition of CCS can increase the average load on the plant and thus its efficiency.[16] Although not yet economically assessed, another interesting possibility involves running the CO_2 capture facility only when excess heat is available (e.g., in summer when district heating load is low), avoiding the large cost of steam for solvent regeneration.[17]

The real-world plant (Twence, the Netherlands) studied in this work produces hot water at 120 °C and has it return from the network at 60 °C. Such elevated temperatures allow the heat to be used for a wider range of purposes and transported over longer distances before becoming too cold due to heat losses. Under such conditions, it is not possible to recover very-low-grade heat from the CO_2 capture system, meaning that CO_2 capture relying on thermal regeneration of the solvent/sorbent becomes more costly as a large fraction of the valuable heat product is lost. CO_2 capture methods that operate on electricity (e.g., vacuum/pressure swing adsorption[18]) would better suit such applications. However, the relatively low CO_2 content in WTE flue gases is not well suited to CO_2 capture processes relying only on a vacuum/pressure swing, resulting in low CO_2 purities in a single-stage process.[12] Two-stage processes can achieve acceptable CO_2 purities, although the deep vacuums required for reasonable efficiency and productivity (e.g., 7.5 kPa[18]) are unlikely to be achievable in practice.[19]

The present study investigates another fully electrified option based on the swing adsorption reactor cluster (SARC) concept[20,21] that maintains efficient operation for more dilute flue gases. SARC uses a combined temperature and vacuum swing through a synergistic combination of heat and vacuum pumps. The vacuum reduces the required temperature swing, ensuring that the heat pump can transfer heat from adsorption to regeneration at a high efficiency.[22] A novel variant of the SARC process, the continuous swing adsorption reactor (CSAR) detailed in the subsequent section, will be investigated. Besides the lower energy penalty, CSAR also allows for flexible operation between electricity to power the heat and vacuum pumps or excess steam available in summer months. As an additional novelty, the present study will quantify the economic benefit of such flexibility to use excess heat, both for the novel CSAR process and the benchmark MEA process.

2. CONTINUOUS SWING ADSORPTION REACTOR (CSAR)

The SARC concept has two primary drawbacks arising from its working principle where both adsorption and regeneration steps take place in each single SARC reactor: (1) the reactor and heat transfer tubes must be heated and cooled together with the sorbent in each temperature swing, increasing the load on the heat pump and (2) sorbent in the lower regions of the reactor experiences a higher pressure in regeneration reducing the achievable sorbent working capacity. These drawbacks are addressed in the CSAR concept presented in the present study. In CSAR, the sorbent is circulated between two reactors for adsorption and regeneration, where lock hoppers are used to facilitate the sorbent transfer across the pressure difference. Although lock hoppers are well-known process units, sorbent circulation between the two CSAR reactors is yet to be demonstrated and presents the most important technical uncertainty for the scale-up of the technology.

Figure 1 shows the working principle of the CSAR concept, with the main equipment being numbered to aid in the process description that follows. Warm flue gas is fed to the adsorber (1) where it is contacted in a counter-current manner with the falling sorbent to capture CO_2. Such an adsorber could be designed as a single fluidized bed with perforated plate separators[20] or as stacked fluidized beds.[23] The heat in the flue gas is transferred to the sorbent for mild preheating before it is circulated to the desorber (3) via the bottom lock hopper (2). The carbonated sorbent flows into the bottom lock hopper under gravity when it is closed to the desorber side and open to the adsorber side. When the lock hopper is full, it is closed to the adsorber side and opened to the desorber side where the vacuum pressures evacuate the sorbent from the lock hopper and initiate the release of CO_2 (and potentially H_2O if the sorbent has also the ability to adsorb H_2O such as polyethylene amine used in the SARC concept demonstration[20]). This gas release then drives the sorbent up into the desorber (2) where heat is supplied by the heat pump (6). The heat pump transfers heat from the exothermic reaction in the adsorber to the endothermic regeneration to drive additional CO_2 and H_2O release (combined temperature and vacuum swing). The released CO_2 and H_2O are extracted at vacuum pressure by the main vacuum pump (7) where water is condensed out and CO_2 is fed to the CO_2 liquefaction section.

The hot regenerated sorbent at the top of the desorber then falls into the top lock hopper (4) that was brought to the same vacuum pressure as the desorber by the small evacuation pump (8). Once the lock hopper is filled, it is closed, and an air valve is opened to repressurize the lock hopper. Once pressurized, the lock hopper is opened to the adsorber side to allow the sorbent to fall into the cooler (5). Here, the heat pump (6) cools the sorbent under a minimal fluidization with air (the small air stream results in minimal losses of CO_2 in the cooler outlet) so that the equilibrium CO_2 partial pressure is reduced when the sorbent is fed to the top of the adsorber.

To further reduce the equilibrium CO_2 partial pressure and ensure maximum CO_2 removal from the flue gas, cooling water at a temperature below that of the heat pump working fluid is used to extract heat at the top of the adsorber (1). From a global energy balance point of view, this heat removal is necessary to balance the heat input from the warm flue gas and the heat generation in the heat pump. In the lower regions of the adsorber, more heat is removed by the heat pump working fluid to limit the temperature rise caused by the exothermic CO_2 and H_2O adsorption.

Another interesting benefit of reducing the sensible heat load and increasing the sorbent working capacity relative to the SARC concept is that the system can also be operated in normal

https://doi.org/10.1021/acs.energyfuels.3c00885
Energy Fuels 2023, 37, 12030−12044

temperature swing adsorption (TSA) mode when cheap heat is available. This would be a relevant case for CHP plants that supply lots of heat in winter, but much less in summer. Thus, in summer, the heat that would otherwise be rejected can be used for CO_2 capture instead of consuming electricity through the heat and vacuum pumps. The present study will quantify the market conditions where a CHP plant will benefit from such seasonal flexibility as opposed to the CSAR concept operating only on electricity throughout the year and conventional MEA CO_2 capture that uses heat to regenerate the solvent.

When operating in TSA mode, a separate desorber with a much smaller cross-sectional area, a taller height, and a smaller heat transfer surface area will be required, mildly increasing the capital cost of the system. The cross-sectional area of the unit must be reduced because it will operate at atmospheric pressure, implying that a dilute fluidization regime is needed to minimize the pressure drop and allow particles to flow from the bottom of the adsorber to the bottom of the desorber. In addition, the higher pressure will strongly reduce the gas volume flowrate relative to CSAR operation. Even though a substantial quantity of heat will be required, the temperature difference between the reactor and the steam available from the WTE plant is relatively high, reducing the heat exchanger surface area required.

Heat removal from the adsorber and cooler remain similar as indicated in Figure 1. However, the heat pump working fluid is no longer compressed, but rather sent to an external fin-fan air cooler to condense the fluid and reject the heat from the exothermic adsorption. The condensed working fluid is then pumped back to the adsorber and cooler to remove heat via evaporation as in the normal CSAR operation. Heat removal by cooling water at the top of the adsorber stays unchanged. The lock hoppers will be bypassed when the unit operates in TSA mode using the dedicated regeneration column because the two reactors will operate at similar pressures.

3. METHODOLOGY

The combined reactor, process, and economic modeling methods used for this study are discussed in three sections below.

3.1. CSAR Reactor Modeling. The CSAR reactor system was modeled under the following simplifying assumptions, which have been experimentally validated for the SARC process[22]

- The reactor can be considered as a series of continuous stirred tank reactors (CSTR). A CSTR is typically a good conceptual representation of well-mixed fluidized beds.
- The reactor contains solid material and gas, the latter of which is represented as a mixture of ideal gases—a valid assumption in this low-pressure system.
- There is thermal and chemical equilibrium between gas and solid. Gas-particle heat transfer is extremely fast in fluidized beds, ensuring thermal equilibrium. Experiments have also shown that reaction rates are fast with the chosen sorbent,[20] closely approximating chemical equilibrium.

3.1.1. Chemistry. Chemical adsorption of CO_2 on the amine (Am) group of the sorbent and physical adsorption of H_2O are described as follows

$$\begin{aligned} &\mathrm{Am} + \mathrm{CO_2(g)} \leftrightarrow \mathrm{AmCO_2}\Delta H = -75\ \mathrm{kJ/mol} \\ &\mathrm{H_2O(g)} \leftrightarrow \mathrm{H_2O(ads)}\Delta H = -43\ \mathrm{kJ/mol} \end{aligned} \tag{1}$$

The equilibrium sorbent loading of CO_2 (q_{CO_2}) [mol/kg] is described in the Toth isotherm as follows[24] (the model coefficients for eqs 2 to 5 are shown in Table 1)

$$q_{\mathrm{CO_2}} = \frac{n_s b p_{\mathrm{CO_2}}}{(1 - (b p_{\mathrm{CO_2}})^t)^{1/t}} \tag{2}$$

$$n_s = n_{s,0} \exp\left(X\left(1 - \frac{T}{T_0}\right)\right) \tag{3}$$

$$b = b_0 \exp\left(\frac{dH}{RT_0}\left(\frac{T_0}{T} - 1\right)\right) \tag{4}$$

$$t = t_0 + \alpha\left(1 - \frac{T_0}{T}\right) \tag{5}$$

Table 1. Model Coefficients for Use in Equations 2 to 5

$n_{s,0}$	X	b_0	dH	t_0	α	T_0
2.146	0.317	38.25	104,581	0.497	1.273	303

For H_2O, a linear fit with the relative humidity (φ) was used.[24]

$$q_{\mathrm{H_2O}} = \begin{cases} 5.69\varphi + 0.2528 \\ 37.66\varphi \text{ if } \varphi < 0.0087 \end{cases} \tag{6}$$

These single-component isotherms can be safely used as no significant multicomponent effects were observed between CO_2 and H_2O for the sorbent used in this study.[24]

3.1.2. Mass and Energy Balances. The following mass balance is solved for gas and solid in each CSTR

$$\begin{aligned} \frac{d\boldsymbol{N}}{dt} &= F^{\mathrm{in}}\boldsymbol{y}^{\mathrm{in}} - F\boldsymbol{y} + \boldsymbol{S}_g^{\mathrm{T}}\boldsymbol{R} \\ \frac{d\boldsymbol{M}}{dt} &= G^{\mathrm{in}}\boldsymbol{x}^{\mathrm{in}} - G\boldsymbol{x} + \boldsymbol{S}_s^{\mathrm{T}}\boldsymbol{R} \end{aligned} \tag{7}$$

Here, $\boldsymbol{N}$ [kmol] is a vector containing the gas holdup of each gas species; F^{in} and F [kmol/s] are the gas flow rates into and out of the CSTR; G^{in} and G [kg/s] are the solids flow rates into and out of the CSTR; $\boldsymbol{y} = \boldsymbol{N}/\mathrm{sum}(\boldsymbol{N})$ [−] is a vector of gas mole fractions (CO_2, H_2O, O_2, and N_2); $\boldsymbol{x} = \boldsymbol{M}/\mathrm{sum}(\boldsymbol{M})$ [−] is a vector of solids mass fractions (Am, $AmCO_2$, and H_2O(ads) in eq 1); $\boldsymbol{M}$ [kg] is a vector of the mass holdup for each solid species; $\boldsymbol{S}$ is the stoichiometric matrix; and $\boldsymbol{R}$ is a vector of chemical reaction rates. The reaction rates are fast so as to satisfy the chemical equilibria in each CSTR, under the validated assumption that chemical equilibrium will be achieved with the selected sorbent.[20]

A single energy balance is solved for each CSTR, assuming thermal equilibrium between the gas and solid phases

$$\begin{aligned} &(\boldsymbol{M}^T\boldsymbol{C}_{\mathrm{p,m,s}} + \boldsymbol{N}^T\boldsymbol{C}_{\mathrm{p,g}})\frac{dT}{dt} \\ &\quad = F^{\mathrm{in}}(\boldsymbol{C}_{\mathrm{p,g}}^{\mathrm{T}}\boldsymbol{y}^{\mathrm{in}})(T_g^{\mathrm{in}} - T) + G^{\mathrm{in}}(\boldsymbol{C}_{\mathrm{p,m,s}}^{\mathrm{T}}\boldsymbol{x}^{\mathrm{in}})(T_s^{\mathrm{in}} - T) \\ &\qquad - \boldsymbol{R}^T\Delta\boldsymbol{H} + Q \end{aligned} \tag{8}$$

Here, $\boldsymbol{C}_{\mathrm{p,m,s}}$ [J/kg·K] and $\boldsymbol{C}_{\mathrm{p,g}}$ [J/kmol·K] are vectors of solids and gas species heat capacities, respectively; T [K] is the reactor temperature; T_g^{in} and T_s^{in} [K] are the inlet temperatures of the gas and solids phases, respectively; $\Delta\boldsymbol{H}$ [J/kmol] is a vector of the

https://doi.org/10.1021/acs.energyfuels.3c00885
Energy Fuels 2023, 37, 12030−12044

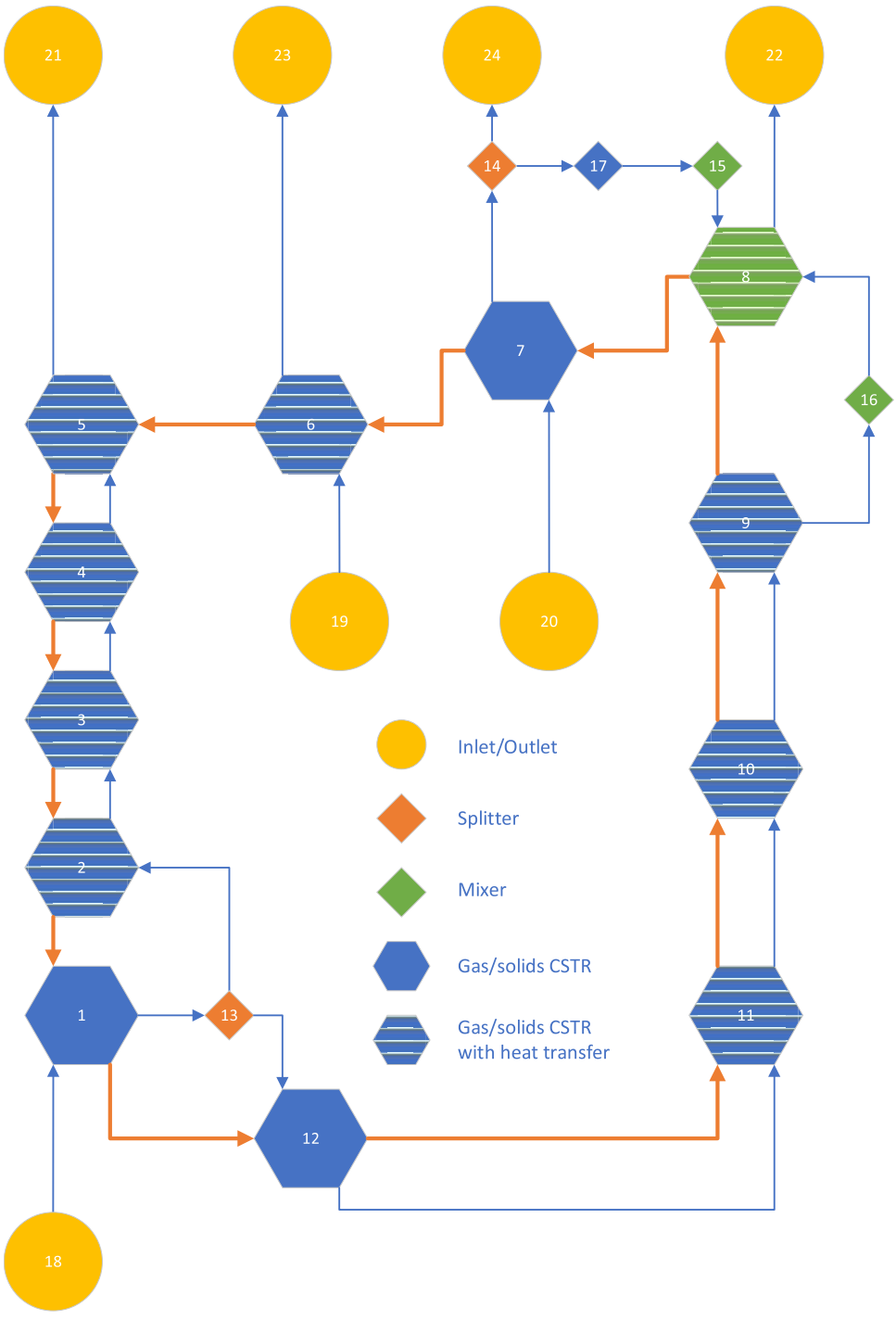

Figure 2. CSTR control volume network used to simulate the CSAR reactor system in VTSA mode.

enthalpies of reaction; and Q [W] is heat added or removed via the heat transfer surfaces. No heat losses to the environment are considered for this low-temperature industrial-scale system. The solids heat capacity was set to 1500 J/kg/K as specified by the supplier.

Heat addition or removal via the heat transfer surfaces is modeled as follows, using an experimentally demonstrated heat transfer coefficient of 400 W/m^2/K[20]

$$Q = UA\Delta T \tag{9}$$

Here, A [m^2] is the total heat transfer surface area, U [W/m^{2}K] is the heat transfer coefficient, and ΔT [K] is the temperature difference between the reactor and the heat transfer fluid. The working fluid temperature is set to a constant value in each reactor, and these temperature assumptions are used in the subsequent process model to calculate the power consumption of the heat pump. The cooling water used at the top of the adsorber (Figure 1) is also assumed to be at a constant temperature (35 °C), even though it would increase by 10 °C between the inlet and the outlet. Hence, the implicit assumption is that the inlet and outlet water temperatures are set below and above the assumed average temperature so as to achieve the total heat transfer rate calculated using the average temperature in eq 9.

https://doi.org/10.1021/acs.energyfuels.3c00885
Energy Fuels 2023, 37, 12030−12044

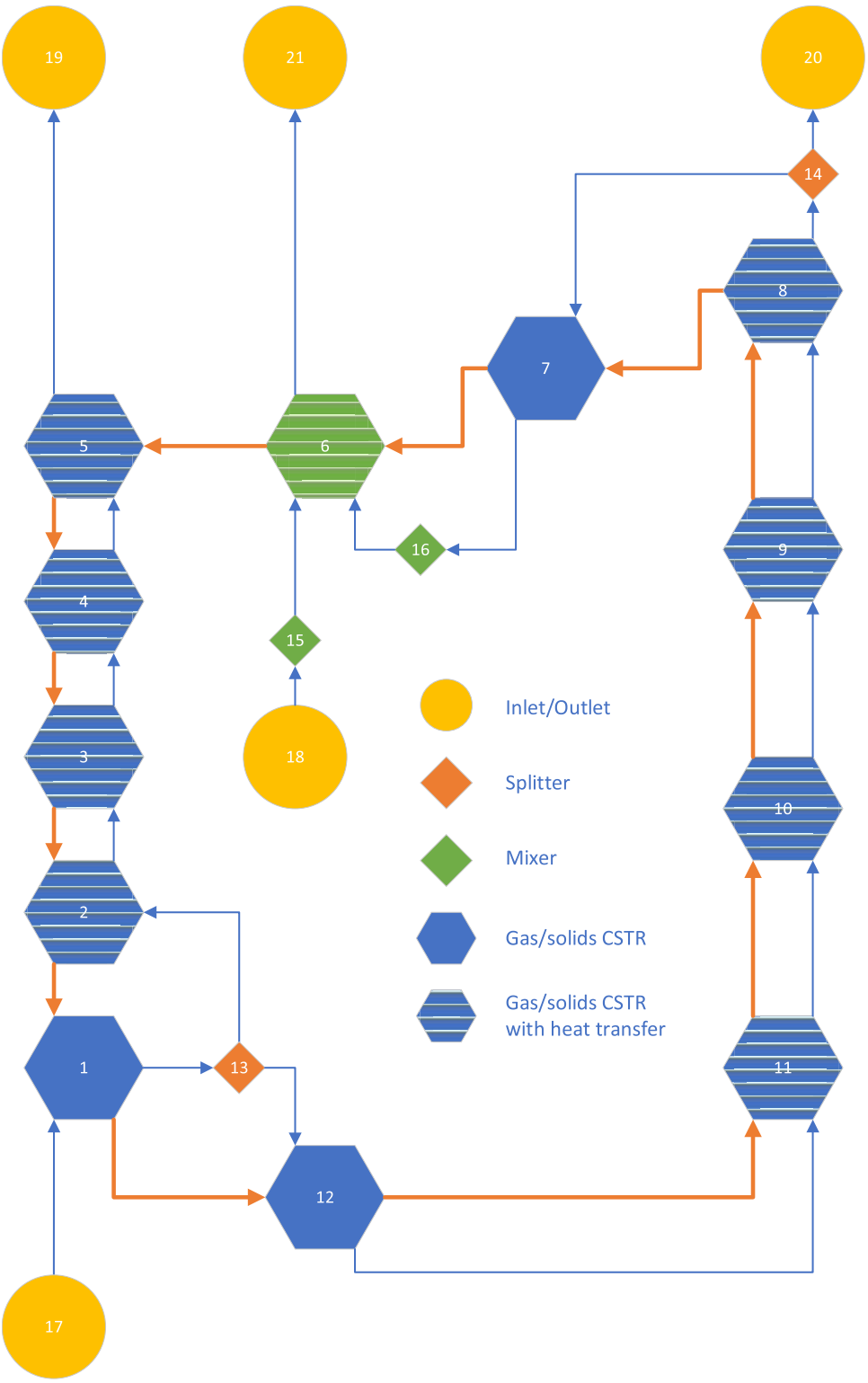

Figure 3. CSTR control volume network used to simulate the CSAR reactor system in TSA mode.

Finally, the ideal gas equation of state is used for the gas, as follows

$$pV_g = \text{sum}(\boldsymbol{N})R_0T \tag{10}$$

Here, p [Pa] is the pressure; V_g [m^3] is the gas volume; and R_0 [J/kmol·K] is the universal gas constant. Appropriate pressure levels are set in each CSTR, imposing atmospheric pressure at the top of the adsorber and 0.2 bar at the top of the desorber. In addition, the pressure is increased linearly toward the bottom of the adsorber and the desorber to account for pressure drops of 0.1 and 0.2 bar in these two reactors, respectively.

3.1.3. Solution Method. The system of equations for the network of coupled CSTRs was solved using ode15s, which is a differential-algebraic equation solver in Matlab, employing default settings. The solution was initialized using constant values in all CSTRs derived from the inlet flue gas stream.

https://doi.org/10.1021/acs.energyfuels.3c00885
Energy Fuels 2023, 37, 12030−12044

3.1.4. CSAR in VTSA and TSA Modes. The CSTR control volumes were linked together as illustrated in Figures 2 or 3, depending on whether the system was operated in VTSA mode (heat and vacuum pumps) or TSA mode (steam).

Both cases featured a counter-current adsorber with heat extraction and a co-current desorber with heat addition. In VTSA mode, the heat is added and removed primarily by the heat pump (using ammonia as working fluid), although additional heat is removed by cooling water at the top of the adsorber (control volume 5 in Figure 2). Additional heat removal is needed to extract heat added to the system by the hot flue gas and the heat pump (which adds more heat than it removes due to the addition of electrical energy). Using cooling water at a lower temperature than the heat pump working fluid at the top of the adsorber reduces the equilibrium CO_2 partial pressure to maximize CO_2 capture from the flue gas. Heat removal from the cooler (control volume 6 in Figure 2) is also completed by the heat pump. The heat pump working fluid evaporation temperature was set to 55 °C, while the cooling water was set to 35 °C (water enters at 30 °C and exits at 40 °C). The amount of cooling water was automatically adjusted in the simulation to satisfy the overall energy balance.

The VTSA desorber operated at a vacuum of 0.2 bar. Although deeper vacuums could bring further cost reductions,[25] this vacuum level was selected to respect practical limits in large-scale vacuum systems.[19] CO_2 capture of 90% was ensured by automatically adjusting the condensation temperature of the heat pump working fluid, controlling the degree of sorbent regeneration achieved. In this case, a temperature of 81.2 °C was needed, while the average temperature of the sorbent was about 6 °C lower to drive the heat transfer.

To realistically represent the undesired gas mixing in the lock hoppers in VTSA mode, the gas streams were split and mixed as illustrated in Figure 2. In the bottom lock hopper (control volume 12), a certain fraction of the cooled flue gas exiting control volume 1 was split off to flow with the sorbent to the desorber. This gas leakage rate was set as the amount of gas that leaks out when the lock hopper is opened to the side of the desorber, assuming that the lock hopper is charged to a solids volume fraction of 0.5 when open to the adsorber side. In the top lock hopper (control volume 7), the gas that is displaced by the sorbent falling into the lock hopper when charged to a solids volume fraction of 0.5 is assumed to leak to the desorber. Both these effects cause a decrease of the CO_2 purity.

During TSA operating mode in summer, heat is still removed by the heat pump working fluid (specified at 50 °C), but rather than being upgraded to a higher temperature by the heat pump compressor for transfer to the desorber, it is rejected at the same temperature in the air cooler. This avoids the use of the heat pump compressor and limits the size of the air cooler due to the significant temperature difference between the working fluid and the ambient. Water is still used to remove heat from the top of the adsorber at a lower temperature of 40 °C (5 °C higher than in VTSA mode to limit the air cooler size with the higher ambient temperature). A smaller desorber, operating at atmospheric pressure and 106.7 °C, is used with a smaller heat transfer surface area due to the availability of steam at 139 °C from the CHP plant. The heat transfer surface area is automatically adjusted in the model to achieve 90% capture. The heat pump, vacuum pumps, and VTSA desorber are idle during this operating mode.

Gas leakage through the bottom lock hopper (control volume 12 in Figure 3) is approximated by calculating the volume of gas that is dragged with the sorbent flowing to the desorber. At the assumed sorbent volume fraction of 0.5, this means that gas and sorbent volume flows are equal. However, it is assumed that the lock hoppers are still active, only being used to limit gas leakage. When the charged lock hopper is opened to the desorber side, there will not be a sufficiently large pressure difference to suck out a significant amount of gas with the sorbent and the only gas leakage would occur from gas mixing caused by the sorbent falling out of the lock hopper. To account for this effect, the gas volume leakage from the adsorber to the desorber, which reduces CO_2 purity, was specified as only half of the sorbent volume flow. This same mechanism was assumed to take place in the top lock hopper (control volume 7): a gas volume flow equal to half the sorbent flow leaks from the desorber to the cooler where the CO_2 is lost to the atmosphere.

The sorbent circulation rate was optimized manually for VTSA and TSA operating modes, minimizing the heat pump power demand in VTSA mode and the desorber heat transfer surface area requirement in TSA mode. VTSA mode required triple the flowrate of TSA mode (300 relative to 100 kg/s of fully regenerated sorbent) because the sorbent working capacity is limited by the relatively small temperature swing that had to be enforced to maximize heat pump efficiency. In TSA mode, on the other hand, the large temperature swing results in a large sensible heat requirement to heat and cool the sorbent, increasing the importance of capturing more CO_2 during each temperature swing by ensuring a larger sorbent working capacity, which allows for a lower circulation rate.

3.1.5. Model Uncertainties. As mentioned earlier, the CSAR model is based on an experimentally validated model of the SARC concept.[22] The CSAR and SARC reactors are both multistage fluidized beds using the same sorbent that is regenerated by a combined temperature and pressure swing. Thus, the following validated assumptions from the SARC model are directly transferrable to the CSAR model:

- The high reactivity of the chosen sorbent makes chemical equilibrium a good assumption.
- Horizontal perforated plates can successfully restrict axial mixing and this effect can be represented by modeling the reactor as CSTRs in series.
- A good heat transfer coefficient of around 400 $W/m^2/K$ can be achieved in the fluidized bed.

However, the conceptual difference between CSAR and SARC introduces three unvalidated assumptions into the model. As outlined below, the associated uncertainties should be relatively small.

- The lock hopper system achieves a steady circulation rate. As mentioned earlier, successful circulation between the CSAR reactors remains to be demonstrated. In addition, there will be a transient element to the circulation from the opening and closing of the lock hoppers. However, an industrial system will employ multiple lock hoppers working in a coordinated manner to transfer a near-steady stream of sorbent between the reactors.
- Counter-current flow can be achieved in the adsorber while still limiting axial mixing. Unlike the SARC reactor where the fluidized sorbent is kept in a single reactor, the sorbent must slowly descend through the CSAR adsorber. Since the holes in the horizontal perforated plates are large enough to allow particles to pass through[22] and the average sorbent velocity is low (0.02−0.03 m/s), such downward particle transport should happen naturally

https://doi.org/10.1021/acs.energyfuels.3c00885
Energy Fuels 2023, 37, 12030−12044

Table 2. Flue Gas Details and Heat Availability from the Simulated CHP Plant

			mol fraction					
flue gas flowrate (kg/s)	temperature (°C)	pressure (kPa)	CO_2	H_2O	O_2	N_2	heat available (MW)	steam temperature (°C)
65.7	164.3	101.4	0.095	0.167	0.076	0.662	62.1	139

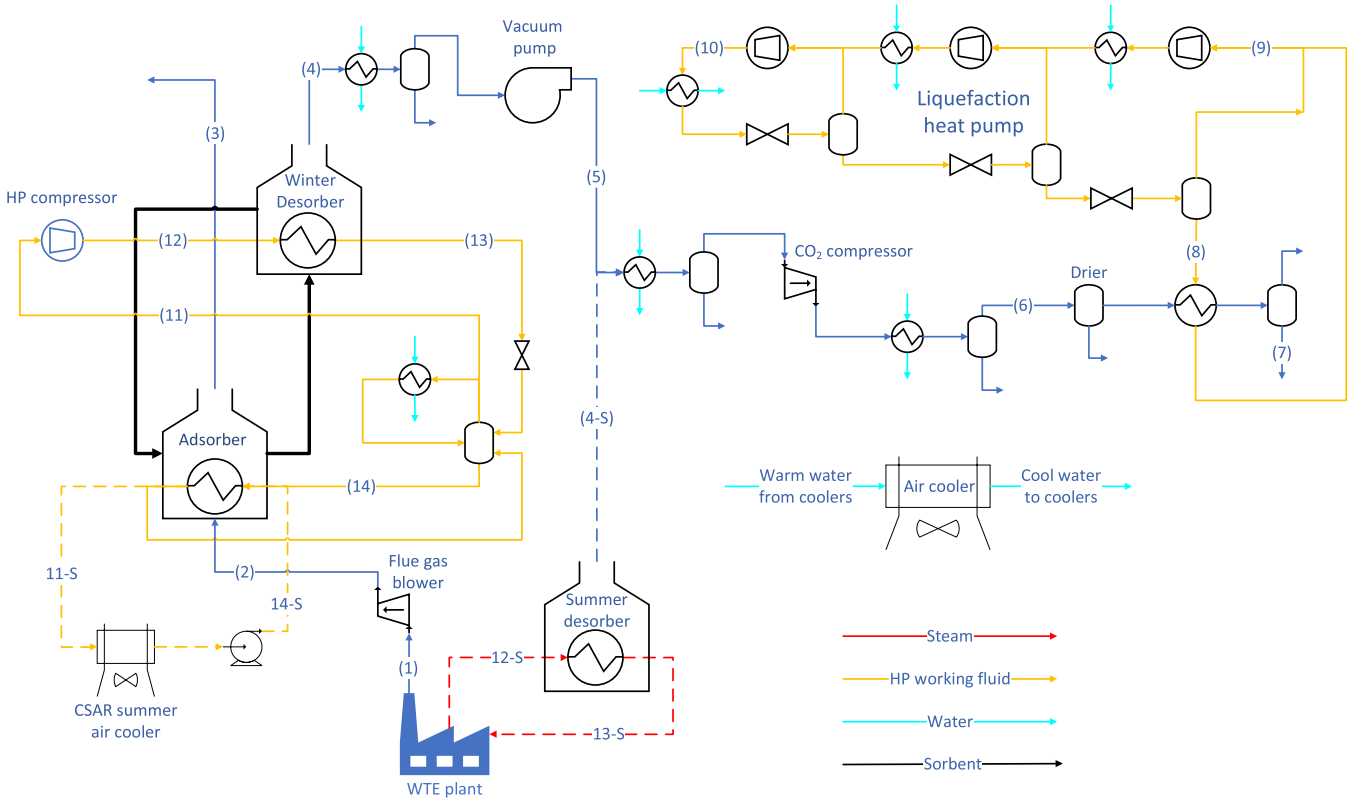

Figure 4. Process scheme for winter and summer mode operation of the CSAR process. Continuous lines represent winter mode, and dashed lines represent summer mode.

under continuous sorbent addition at the top and extraction at the bottom.

- Successful TSA operation in summer mode. The SARC validation experiments always used a vacuum in desorption, so desorption via pure TSA was not tested. However, the sorbent used in the experiments was originally developed for a pure TSA application, and earlier SARC proof-of-principle experiments showed predictable behavior in pure TSA operation.[26]

Another important uncertainty is related to long-term sorbent stability. Good chemical stability has been demonstrated over 800 cycles in a dual fluidized bed laboratory setup,[27] and a low attrition index of 2.5 was measured in a standardized test,[27] which compares favorably to commercial fluidized bed catalysts.[28] CSAR may further improve sorbent longevity because it operates under gentler fluidization (without cyclones) and lower desorption temperatures than the dual circulating fluidized bed arrangement usually considered for pure temperature swing adsorption applications. Lower desorption temperatures will be beneficial for long-term stability because PEI sorbents exhibit a strong thermal deactivation mechanism,[29] although functionalization with 1,2-epoxybutane significantly increases the feasible operating temperature.[30]

3.2. Process Modeling. The WTE plant flue gas and heat availability were provided by the Twence CHP plant in the Netherlands as summarized in Table 2. CO_2 capture from this flue gas was modeled for the CSAR process and an MEA benchmark as outlined in the two subsections below.

3.2.1. CSAR Process Model. Two process schemes for capturing CO_2 by CSAR integration to the CHP plant are developed and modeled in Aspen Plus for winter and summer operation (both modes depicted in Figure 4 and Table 4) under the assumptions detailed in Table 3.

Table 3. Key Assumptions in the CSAR Process Simulations

parameter	values	units
CO_2 & NH_3 compressor isentropic efficiency	0.85	
CO_2 & NH_3 compressor mechanical efficiency	0.95	
number of stages in CO_2 liquefaction	3	
intercooling temperature	30	°C
number of stages in refrigeration cycle	3	
targeted CO_2 liquefaction pressure	33.8	bar
pressure drop in heat exchanger	1% of inlet pressure	
winter air temperature	7.5	°C
summer air temperature	15	°C
absorber pressure drop	0.1	bar
flue gas inlet temperature	164.3	°C
capture ratio	90	%
regeneration pressure in winter mode	0.2	bar
regeneration pressure in summer mode	1	bar

https://doi.org/10.1021/acs.energyfuels.3c00885
Energy Fuels 2023, 37, 12030−12044

Table 4. Stream Data for the CSAR Process Simulations According to the Numbering in Figure 2

				(mol fraction)				
stream number	pressure (bar)	temperature (°C)	mass flowrate (kg/s)	N_2	CO_2	H_2O	O_2	NH_3
flue gas								
1	1.00	164.3	65.72	0.662	0.095	0.167	0.076	
2	1.10	177.2	65.72	0.662	0.095	0.167	0.076	
winter mode								
3	1.00	47.5	50.86	0.854	0.012	0.036	0.098	
4	0.20	74.1	14.73	0.011	0.380	0.608	0.002	
5	1.01	99.0	9.25	0.026	0.899	0.0721	0.004	
6	33.81	31.7	8.97	0.028	0.967	0.002	0.004	
7	33.47	−28.0	8.93	0.026	0.970		0.004	
8	1.10	−31.0	1.99					1.000
9	1.10	9.2	2.11					1.000
10	11.82	98.9	2.52					1.000
11	23.21	54.8	21.57					1.000
12	42.82	115.0	25.34					1.000
13	42.82	81.1	25.34					1.000
14	23.21	54.8	21.57					1.000
summer mode								
3	1.00	49.3	51.87	0.836	0.011	0.061	0.095	
4-S	1.00	106.6	13.76	0.004	0.420	0.575	0.001	
6	33.81	31.7	8.84	0.009	0.988	0.002	0.001	
7	33.47	−28.0	8.84	0.009	0.990		0.001	
8	1.10	−31.0	1.99					1.000
9	1.00	9.7	2.12					1.000
10	11.83	98.9	2.52					1.000
11-S	20.41	50.2	29.47					1.000
14-S	20.51	50.2	29.47					1.000

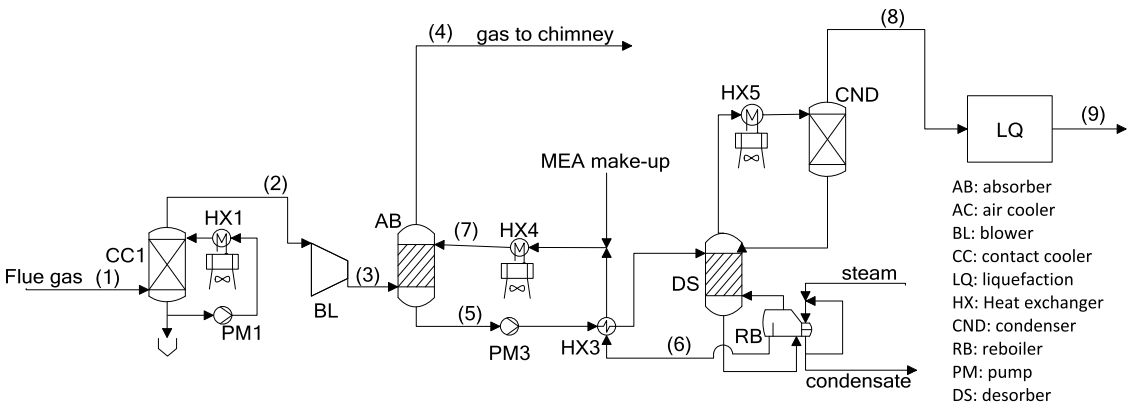

Figure 5. MEA capture plant process scheme.

In winter mode, the flue gas from the CHP plant (stream 1) is fed to the adsorber via a blower (stream 2) to overcome the pressure drop in the adsorber. The flue gas is contacted in a counter-current mode in the adsorber to capture CO_2 from the flue gas and the CO_2 lean stream (3) is vented to the atmosphere. A combined temperature and vacuum swing is used in the desorber to release the captured CO_2 (stream 4) which is fed to the multistage compressor (stream 5) after being brought to atmospheric pressure by the vacuum pump. The compressed CO_2 stream (stream 6) is dried to prevent ice formation and fed to the cryogenic section to liquify the captured CO_2 (stream 7). The cooling duty required for liquefaction is supplied by a 3-stage refrigeration cycle using NH_3 as a working fluid. Heat is continuously removed from the adsorber and the cooler via another NH_3 heat pump by evaporating the working fluid (stream 14) and added to the desorber by condensing the working fluid (stream 12).

In summer mode, the desorber is operated under TSA mode using the available steam (stream 12-S) from the CHP plant that would otherwise have to be rejected due to a lack of heat demand in summer. The temperature in the adsorber is still controlled by extracting heat by evaporating the heat pump fluid (stream 11-S). In this case, however, the heat from stream 14-S is rejected to air in an additional air cooler to condense the working fluid before it is sent back to the adsorber. As summer mode is operated under TSA mode under atmospheric pressure, captured CO_2 (stream 4-S) is fed directly to the compression section, bypassing the vacuum pump (Table 4).

3.2.2. MEA Process Model. One process scheme for capturing CO_2 by MEA integration to the CHP plant is developed and

https://doi.org/10.1021/acs.energyfuels.3c00885
Energy Fuels 2023, 37, 12030−12044

Table 5. Stream Data for the MEA Capture Plant Simulations According to the Numbering in Figure 5

				(mol fraction)				
stream number	pressure (bar)	temperature (°C)	mass flowrate (kg/s)	N_2	CO_2	H_2O	O_2	MEA
flue gas								
1	1.00	164.3	65.72	0.662	0.095	0.167	0.076	
2	0.96	40.0	61.66	0.733	0.105	0.078	0.084	
3	1.10	50.1	61.66	0.733	0.105	0.078	0.084	
4	1.01	52.5	54.12	0.780	0.010	0.121	0.089	
5	1.05	53.8	288.79		0.054	0.882		0.113
6	1.83	115.6	279.89		0.037	0.885		0.113
7	1.50	39.7	281.25		0.036	0.887		0.112
8	1.50	39.8	8.96		0.950	0.050		
9	33.47	−28.0	8.70		1.000			

modeled in Aspen Plus. The scheme is shown in Figure 5, while the assumptions are the same as those outlined in Table 3.

The chemical absorption of CO_2 of the MEA-based capture plant is an electrolyte process, so a suitable thermodynamic model is required to describe the process. A thermodynamic model available in Aspen Plus was used; it is based on the ELECNRTL property model and allows rate-based calculation.

The flue gas from the CHP plant is fed at the bottom of the contact cooler column in which an air-cooled water flux is distributed at the top of the column to achieve a final temperature of the flue gas of about 40 °C. This decreases the volumetric flow rate of the gas and brings the temperature to the proper one to be processed in the absorber that it is reached via a blower to overcome the pressure drops. The flue gas is treated in a counter-current mode in the absorber, which is 8.2 m in diameter with a packing height of 18 m, to capture CO_2 by a downward-flowing lean CO_2-loaded solvent. Here occurs the exothermic chemical absorption of CO_2. The solvent at the bottom of the absorber is a CO_2-rich stream pumped to a recuperative heat exchanger, increasing the temperature before reaching the desorber. The solvent regeneration occurs by reversing the chemical reaction using heat added via steam condensation in the reboiler, with the heat input being adjusted to achieve a 90% capture ratio. From the bottom of the desorber, the hot CO_2-lean stream is sent to the recuperative heat exchanger. The CO_2 exits from the top of the desorber and is cooled in a condenser that eliminates most of the H_2O. Subsequently, the CO_2 is liquified using the same process as in CSAR. The summary of stream data is provided in Table 5.

The MEA process is investigated in conventional mode where it operates throughout the year and in a flexible mode where it operates only in summer when heat is available for free. Unlike CSAR that can continue operations during winter on electrical energy, such idling during winter months will increase the levelized capital cost in exchange for avoiding the cost of consuming the heat product of the plant.

3.3. Economic Assessment. The economic assessment was completed using the open Standardized Economic Assessment (SEA) tool,[31] with the full economic assessment spreadsheets available online[a] and as Supporting Material. Details can be found in the SEA User Guide.[32]

The SEA tool is a bottom-up economic assessment framework where capital costs are assessed in detail, largely using correlations from Turton et al.[33] A correlation from Woods[34] was used for the vacuum pump. The resulting costs were then added up to yield the bare erected cost of the plant and increased using various factors to the total overnight cost as outlined in Table 6. All costs are adjusted for currency, year, and location.

Table 6. Conversion of Total Installed Costs of All Major Equipment to Total Capital Requirement for Constructing the Plant

bare erected cost (BEC)	sum of all installed equipment costs
Process contingency (PSC)	20% of BEC for CO_2 capture units, 0% otherwise
Engineering procurement and construction (EPC)	8% of BEC
Project contingency (PTC)	15% of (BEC + PSC + EPC)
Total plant costs (TPC)	BEC + PS + EPC + PTC
Owner's cost (OC)	15% of TPC
Total overnight costs (TOC)	TPC + OC

All relevant operating costs are added and a cash flow analysis is completed to find the levelized cost of liquified CO_2, i.e., the CO_2 value needed to reach a net present value of zero at the chosen discount rate, plant lifetime, and construction period. In other words, the liquid CO_2 stream is treated as a revenue source that recuperates the expense of building and operating the CO_2 capture and liquefaction facilities (assuming that the plant will receive payments for capturing biogenic CO_2 for negative emissions). No CO_2 transport and storage costs are included as this will be highly case-dependent for such small facilities. For example, the real-world plant simulated in this work plans to sell CO_2 to nearby greenhouses at a profit. The main economic assumptions are detailed in Table 7.

Table 7. Key Assumptions in the Economic Assessment

currency, year, location	Euros (€), 2020, North Europe
discount rate	8%
economic lifetime	25 years
construction period	2 years
first year and general capacity factor	65% and 90%
fixed operating costs	4.5% of TOC per year
base case electricity and heat costs	60 and 30 €/MWh
sorbent cost	15 €/kg
solvent cost	2 €/kg

Fixed operating costs account both for routine maintenance and insurance. For the flexible CSAR and MEA plants, it was assumed that this cost is only 3% of TOC per year for all of the plant components that are only used for half the year. It can be reasonably assumed that these components will require considerably less maintenance than components that are used throughout the year.

Electricity and heat costs are highly case-dependent and are therefore varied in a sensitivity analysis presented in Section 4.

https://doi.org/10.1021/acs.energyfuels.3c00885
Energy Fuels 2023, 37, 12030−12044

Table 8. Electricity Consumption from the Three Different Plants during Summer and Winter (kW)

	CSAR		Flex CSAR		MEA	
Item	winter	summer	winter	summer	winter	summer
blowers	1007.6	1007.6	1007.6	1007.6	682.0	682.0
heat pump	2772.9	2772.9	2772.9	0.0	0.0	0.0
vacuum pumps	1400.4	1400.4	1400.4	0.0	0.0	0.0
CO_2 liquefaction	3620.8	3620.8	3620.8	3565.1	2954.9	2954.9
air coolers	257.1	556.1	257.1	782.8	591.1	1094.8
MEA pumps	0	0	0	0	402.5	402.5
water pumps	4.5	4.5	4.5	4.5	73.0	71.1
total	9063.3	9362.4	9063.3	5360.0	4703.5	5205.3

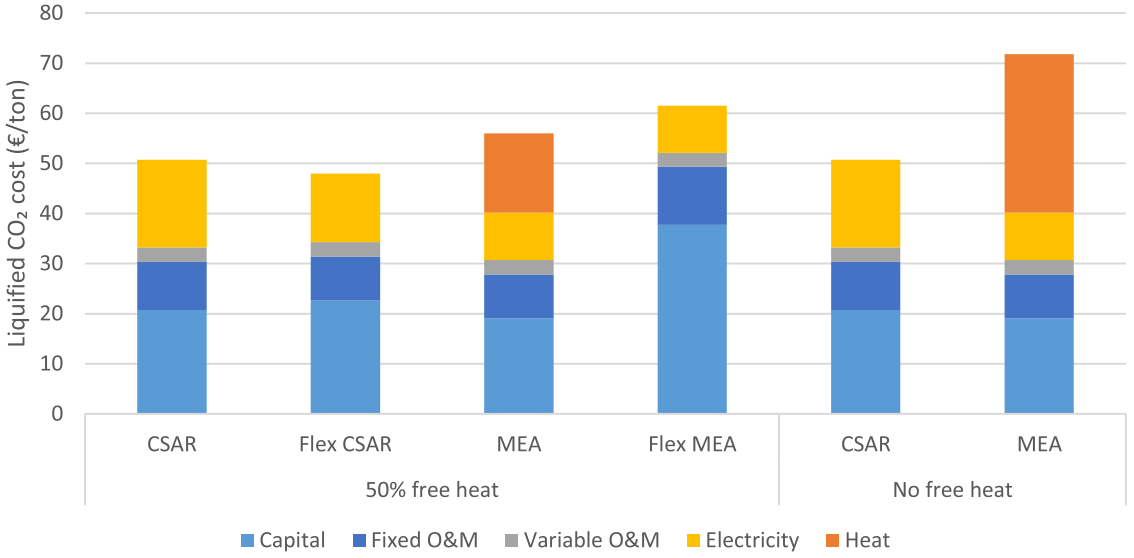

Figure 6. Breakdown of liquified CO_2 costs for the different technologies assuming electricity and heat prices of 60 and 30 €/MWh, respectively.

4. RESULTS AND DISCUSSION

Results are presented and discussed in three sections: (1) technical results, (2) economic results, and (3) mapping the competitiveness of the three investigated plant configurations across different electricity and heat prices.

4.1. Technical Results. Table 8 shows the technical performance of the three plants. The blower consumption in the CSAR plants is considerably higher than in MEA due to the conservatively high pressure drop assumed. Experimental tests have shown rapid CO_2 adsorption[20] that should allow for an attractively short and/or dilute adsorber, but the counter-current fluidized bed operation of CSAR may require a taller bed with a large pressure drop. Experimental demonstration is required before more optimistic assumptions can be considered.

Aside from CO_2 liquefaction, the heat and vacuum pump used to regenerate the sorbent represents the main power consumption in the CSAR concept, whereas the MEA concept requires 33 MW of heat (more than half of the CHP plant's heat output) to regenerate the solvent. Due to the efficiency of the heat pump, the electrical energy required for sorbent regeneration in CSAR is almost 8 times lower than the thermal energy needed in MEA. Even though electricity is more valuable than district heat, this large difference in energy consumption promises a considerable economic benefit from CSAR. Coincidentally, Flex CSAR also uses 33 MW of heat for sorbent regeneration in summer, but this heat is assumed to be available at no cost. The sorbent used in CSAR has a lower regeneration enthalpy than MEA, but a large amount of water is also adsorbed from the flue gas and CSAR does not use any heat integration between the warm sorbent from the desorber and cold sorbent from the adsorber, bringing the total heat duty to a similar level as MEA.

CO_2 liquefaction costs are higher for CSAR than MEA due to the lower CO_2 purity (~97% relative to 100% for MEA) and the slightly pressurized state (1.5 bar in this case) at which the MEA process produces CO_2. Flex CSAR achieves 99% purity in summer mode due to avoiding the gas leakage associated with pressure changes in the lock hoppers during conventional CSAR operating mode.

The greatest difference between winter and summer power consumption is related to air coolers. During summer, much greater cooler fan consumption is required due to the higher ambient temperature assumed (15 °C in summer vs 7.5 °C in winter). The MEA process needs to reject the most heat, resulting in the largest air cooler fan power consumption.

Water pump power consumption is higher for MEA due to greater heat rejection requirements. During summer operation, Flex CSAR reduces water consumption because heat is rejected directly from the ammonia circuit in the adsorber and the cooler.

4.2. Economic Results. The comparison between CSAR and the MEA benchmark is shown in Figure 6. The full details behind this figure can be viewed online[b] or in the Supporting Material in the open access economic assessments completed with the SEA tool.

The figure differentiates cases with and without large amounts of heat that cannot be sold in the summer. Such free heat is

https://doi.org/10.1021/acs.energyfuels.3c00885
Energy Fuels 2023, 37, 12030−12044

positive for processes relying on a temperature swing such as MEA and the flexible CSAR configuration. Figure 6 shows that the MEA process returns only slightly higher costs for capturing and liquifying CO_2 than the CSAR configurations when it can operate on free heat 50% of the time. However, when no free heat is available, it becomes 40% more expensive than CSAR due to the large cost of heat for regenerating the solvent.

The flexible CSAR configuration returns the lowest cost when free heat is available. Due to the assumption that fixed O&M is reduced by a third on the equipment that is only used for half the year; the sum of capital and fixed O&M costs is similar between the CSAR and Flex CSAR configurations. Thus, the reduced electricity consumption by the Flex CSAR configuration during summer months when it runs on free heat significantly reduces overall costs. If O&M costs are not reduced on equipment used only half the year, liquified CO_2 costs increase by 1.7 €/ton.

Operating the MEA benchmark in a flexible mode where it is idled during winter months does not appear to be profitable if free heat is available only 50% of the year. The reduced capital utilization causes the levelized capital costs to double and the fixed O&M cost to increase by a third. These increases exceed the benefits of avoiding the consumption of heat valued at 30 €/MWh.

The MEA process returns lower capital costs than the CSAR options. Figure 7 illustrates that this is mainly due to the avoidance of the additional turbomachinery involved in the heat and vacuum pumps (included in the "Other equipment" category). The CSAR plants also involve significantly higher heat rejection costs, mainly due to the added costs involved in cooling the vacuum pressure stream exiting the desorber. Furthermore, the higher CO_2 purity and pressure delivered by MEA also reduce CO_2 liquefaction compressor costs relative to CSAR. On the other hand, CSAR brings large savings on vessels and heat integration, despite its larger desorber. The three main reasons for the substantially lower cost of CSAR in this category are: (1) CSAR uses carbon steel equipment, whereas MEA uses stainless steel clad vessels and stainless steel heat exchangers to resist corrosion from the MEA solvent, (2) CSAR avoids the recuperator which imposes a substantial cost in the MEA plant due to the large MEA flowrate and the narrow temperature approach in this heat exchanger, and (3) CSAR processes the hot flue gas directly, whereas MEA employs an additional direct contact cooler to cool the flue gas. Finally, the flexible CSAR configuration faces higher capital costs due to the need for the extra desorber and air cooler.

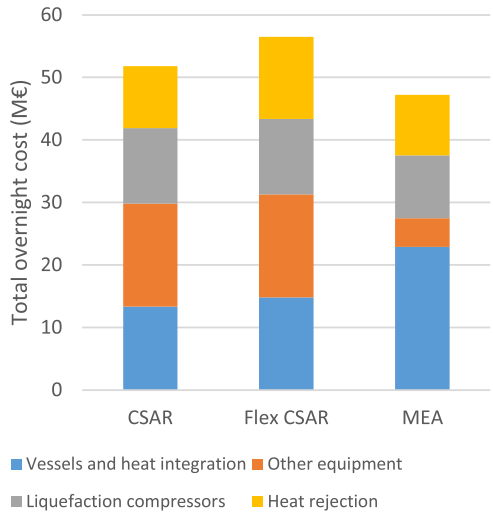

Figure 7. Capital cost breakdown of the three plants. "Other equipment" comprises blowers and flue gas coolers for MEA, while the heat and vacuum pump costs dominate this category for the CSAR plants.

Significant uncertainty exists regarding the costs of the large-scale heat and vacuum pumps employed in the CSAR concept. Figure 8 explores this uncertainty, revealing that changes to the costs of these units have a moderate but significant effect on the liquified CO_2 cost from the CSAR plant. Even so, large cost escalations (well beyond 50%) will be required to drive the cost of CSAR above that of MEA, even in the case where free heat is available for half the year.

4.3. Sensitivity to Electricity and Heat Prices. The value of the heat and electricity sold by a CHP plant can vary strongly from case to case. For example, when the CHP plant competes with natural gas heating, a good benchmark could be natural gas prices (with an appropriate addition for CO_2 emissions). Comparative costs between the distribution networks of hot water and natural gas represent another important factor. When the CHP plant competes with electric heating, heat may have a similar value to electricity. For systems where electric load peaks in the heating season, CHP can bring large added benefits by reducing the costly electricity distribution capacity required. Heat pumps complicate this comparison further by trading lower electricity consumption for higher capital costs.

CO_2 capture retrofits that consume some of the plant's electricity or heat production introduce additional complexity in this valuation exercise. For example, when a CHP plant installs CO_2 capture that consumes more than half the heat output during the heating season, most existing heat customers need to transition to a different solution (or additional CHP capacity needs to be built). Such a transition may involve substantial additional capital expenses and an under-utilization of the existing hot water distribution system, leading to a high cost of the heat consumed by the CO_2 capture plant.

For these reasons, the 30 €/MWh heat price assumed in the previous section may be conservatively low. It represents natural gas at a price of 5.5 €/GJ and a CO_2 price of 50 €/ton and ignores the capital cost implications discussed in the previous paragraph. As shown in Figure 9 (left), higher heat prices strongly increase the cost of the MEA benchmark, whereas CSAR is unaffected. Such cases where the loss of heat supply capacity is very costly present a strong business case for electrically powered CO_2 capture technologies like CSAR.

Elevated electricity prices affect CSAR more than MEA, but the difference is relatively small, given that MEA also consumes a substantial amount of electricity for running blowers, pumps, air coolers, and CO_2 liquefaction compressors (Table 8). Higher electricity prices are possible when electricity from the CHP plant is used in a decentralized manner, avoiding some electricity transmission and distribution capacity from the centralized grid.

The regions where CSAR and MEA are the preferred solutions are indicated by the solid lines in Figure 10. The availability of free heat benefits the MEA benchmark, even when the flexible CSAR configuration is employed. This is shown by MEA being competitive at higher heat prices with 50% free heat than when no free heat is available. In general, MEA needs unrealistically low heat prices to be the preferred solution, especially when no free heat is available.

A more advanced piperazine amino-methyl-propanol (PZ/AMP) solvent achieving 25% lower energy demand and 5%

https://doi.org/10.1021/acs.energyfuels.3c00885
Energy Fuels 2023, 37, 12030−12044

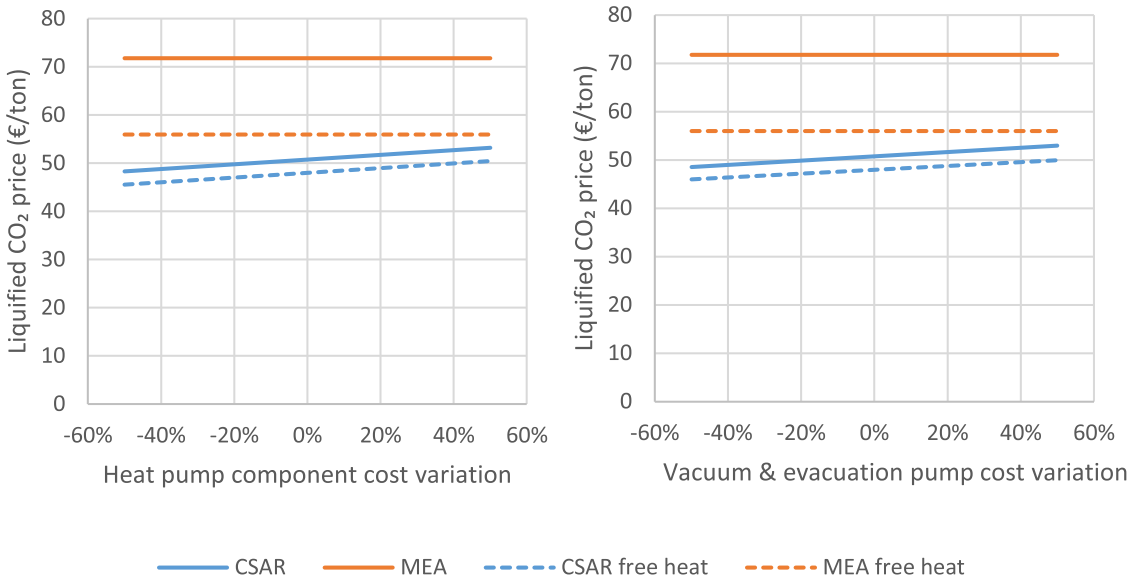

Figure 8. Effect of CSAR heat and vacuum pump costs on its competitiveness against the MEA benchmark. The heat pump includes the heat pump compressor, the NH_3 drum, and the heat exchanger surfaces inside the reactors.

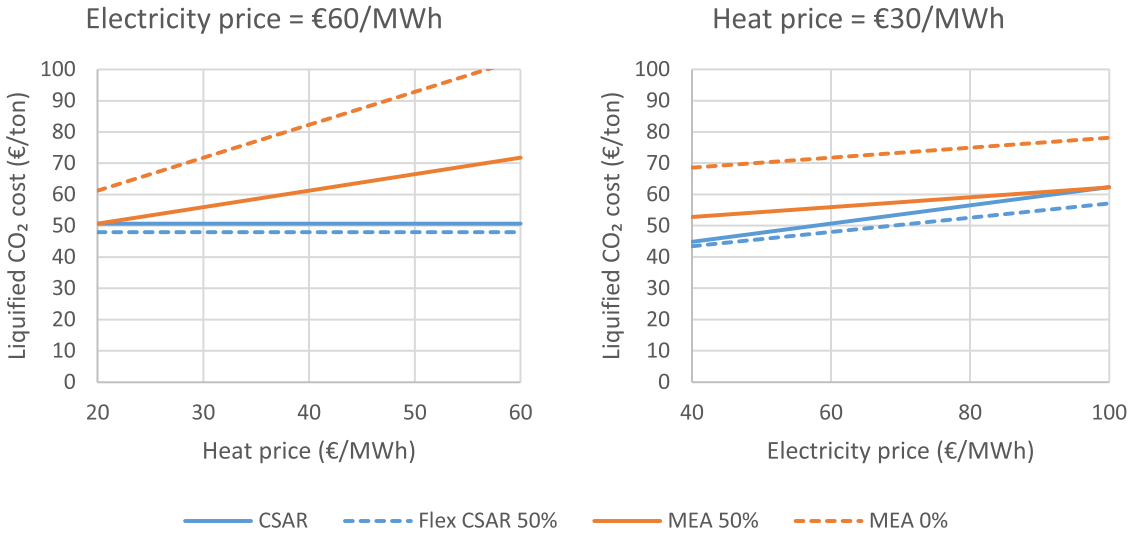

Figure 9. Effect of heat and electricity prices on the liquified CO_2 costs resulting from the CSAR and MEA plants considered in this study. 50 and 0% in the legend refer to the fraction of free heat available during the year.

lower capital costs than MEA[35] is also included in Figure 10 (dashed lines) as a more competitive benchmark. In this case, CSAR requires considerably higher heat prices to outcompete the solvent technology. When no free heat is available, CSAR will remain the preferred solution in most cases as the heat price required by PZ/AMP to compete remains unrealistically low. However, when 50% free heat is available, PZ/AMP presents a more attractive solution that may outcompete CSAR in some cases. For example, Figure 10 (right) shows that CSAR and PZ/AMP present equivalent economic performance with the base case heat (30 €/MWh) and electricity (60 €/MWh) prices assumed in this study.

5. CONCLUSIONS

Combined heat and power (CHP) plants often use difficult-to-combust fuels like waste and low-grade biomass because they can afford to use simple and inefficient power cycles. This raises the possibility of achieving negative CO_2 emissions via CO_2 capture and utilization or storage (CCUS). When heat is the primary valuable product produced by the plant, conventional CO_2 capture processes consuming a large quantity of heat become less attractive unless a productive use can be found for the large amount of very-low-grade heat (typically below 50 °C) rejected from the CO_2 capture facility. Thus, processes capturing CO_2 using electrical power only may be better candidates for enabling CCUS from CHP plants.

The present study investigated the prospects of the novel continuous swing adsorption reactor (CSAR) that captures CO_2 using combined vacuum and temperature swing adsorption (VTSA) driven by heat and vacuum pumps. CSAR consumes only electrical power and could also be configured to run on heat from the plant when excess heat is available for free, especially during summer months. The CSAR concept running on electricity throughout the year, a flexible CSAR configuration that switches to running on free heat during the summer, and a conventional monoethanolamine (MEA) benchmark were

https://doi.org/10.1021/acs.energyfuels.3c00885
Energy Fuels 2023, 37, 12030−12044

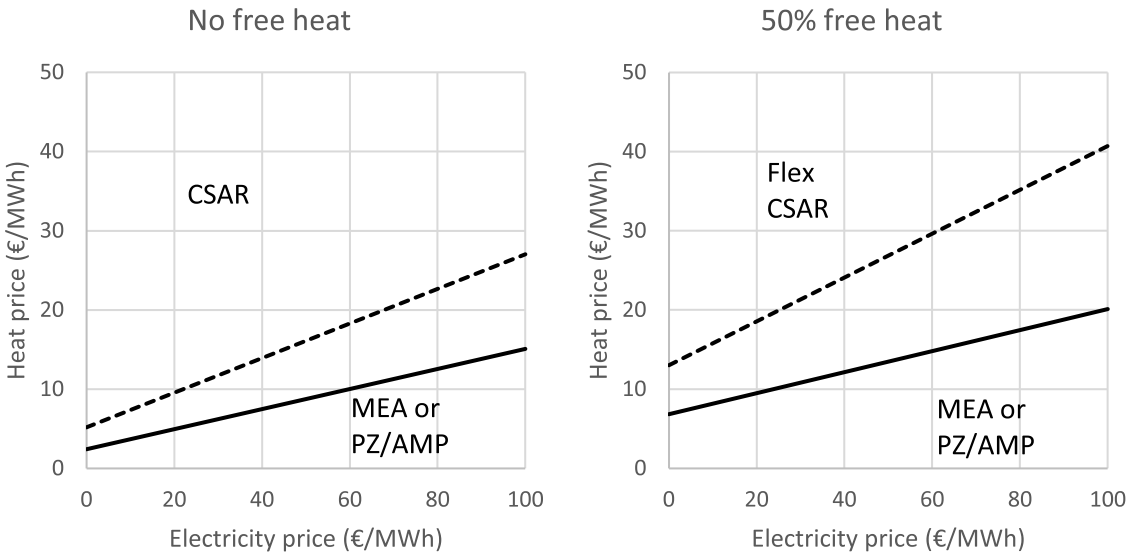

Figure 10. Combinations of electricity and heat prices where MEA (solid line) and CSAR are the preferred options with and without the availability of free heat during summer months. Approximated performance of an advanced PZ/AMP solvent (dashed line) is also included as a stricter benchmark.

compared in a techno-economic analysis to map out the prospects of CSAR.

Without the availability of free heat during the summer, CSAR is clearly the superior solution, as MEA consumes most of the plant's heat output for CO_2 capture. To compete with CSAR, MEA would need unrealistically low heat prices of 9−15 €/MWh when electricity costs 50−100 €/MWh, although an advanced PZ/AMP solvent benchmark increases this range to 16−27 €/MWh. If free summer heat is available, MEA becomes considerably more attractive, doubling breakeven heat prices in an example where free heat is available for half the year. However, the flexible CSAR configuration also improves the competitiveness of CSAR in this scenario, lowering MEA breakeven heat prices to 13−20 €/MWh (27−41 €/MWh against the PZ/AMP benchmark) with electricity prices of 50−100 €/MWh.

In most cases, CHP plants would sell heat for substantially higher prices than those needed for a competitive MEA process (mentioned above), although advanced solvents offer stronger competition, especially when a significant amount of free heat is available. When considering retrofits to existing plants, the costs of solvent-based solutions would be even higher because of the capital cost implications of supplying existing heat customers with an alternative heat supply when most of the CHP plant's heat is consumed for CO_2 capture. For these reasons, the CSAR concept appears to be a highly promising technology for application to CHP plants, and investments in dedicated experimental demonstration of the concept can be recommended.

■ ASSOCIATED CONTENT

Supporting Information

The Supporting Information is available free of charge at https://pubs.acs.org/doi/10.1021/acs.energyfuels.3c00885.

Full economic assessment of the CSAR cases and the MEA benchmark (ZIP)

■ AUTHOR INFORMATION

Corresponding Author

Abdelghafour Zaabout − *Process Technology Department, SINTEF Industry, Trondheim 7034, Norway; ACER CoE Center, University Mohammed 6 Polytechnic, Ben Guerir 43150, Morocco;* orcid.org/0000-0002-7468-8050; Phone: +4793008204; Email: abdelghafour.zaabout@sintef.no

Authors

Schalk Cloete − *Process Technology Department, SINTEF Industry, Trondheim 7034, Norway*

Chaitanya Dhoke − *Process Technology Department, SINTEF Industry, Trondheim 7034, Norway;* orcid.org/0000-0001-5580-1962

Davide Bonalumi − *Department of Energy, Politecnico di Milano, Milano 20156, Italy;* orcid.org/0000-0002-4116-0532

John Morud − *Process Technology Department, SINTEF Industry, Trondheim 7034, Norway*

Antonio Giuffrida − *Department of Energy, Politecnico di Milano, Milano 20156, Italy*

Matteo Carmelo Romano − *Department of Energy, Politecnico di Milano, Milano 20156, Italy*

Complete contact information is available at: https://pubs.acs.org/10.1021/acs.energyfuels.3c00885

Notes

The authors declare no competing financial interest.

■ ACKNOWLEDGMENTS

This study was partly funded under the Climit-Demo project "Verification and demonstration of an advanced adsorption reactor for cost-effective CO_2 capture" with grant number 621172. The internal financial support from SINTEF for preparing the draft is also acknowledged. The authors also acknowledge all valuable information provided by Henk Fikkert about Twence Waste-to-Energy plant in the Netherlands.

LIST OF ACRONYMS

BECCS = bioenergy CO_2 capture and storage
CCS = CO_2 capture and storage
CHP = combined heat and power
CSAR = continuous swing adsorption reactor
CSTR = continuous stirred tank reactor
MEA = monoethanolamine
O&M = operating and maintenance
SARC = swing adsorption reactor cluster
SEA = standardized economic assessment
TOC = total overnight cost
TSA = temperature swing adsorption
VPSA = vacuum pressure swing adsorption
WTE = waste-to-energy

ADDITIONAL NOTES

[a]https://bit.ly/3yYVSZ5
[b]https://bit.ly/3yYVSZ5

REFERENCES

(1) UNFCCC. Historic Paris Agreement on Climate Change 2015. Available from: https://unfccc.int/process-and-meetings/the-paris-agreement/the-paris-agreement.
(2) IPCC. *Fifth Assessment Report: Mitigation of Climate Change*, Intergovernmental Panel on Climate Change, 2014.
(3) IEA. *CUS in clean energy transitions, in Energy Technology Perspectives*, Special report on carbon capture utilization and storage; International Energy Agency, 2020.
(4) IPCC. *Global Warming of 1.5 °C*, Intergovernmental Panel on Climate Change, 2018.
(5) Gapminder. Global income mountains 2022. Available from: https://www.gapminder.org/fw/income-mountains/.
(6) Fajardy, M.; Dowell, N. M. Can BECCS deliver sustainable and resource efficient negative emissions? *Energy Environ. Sci.* **2017**, *10*, 1389−1426.
(7) Dong, J.; Tang, Y.; Nzihou, A.; et al. Comparison of waste-to-energy technologies of gasification and incineration using life cycle assessment: Case studies in Finland, France and China. *J. Cleaner Prod.* **2018**, *203*, 287−300.
(8) Roussanaly, S.; Ouassou, J. A.; Anantharaman, R.; et al. Impact of Uncertainties on the Design and Cost of CCS From a Waste-to-Energy Plant. *Front. Energy Res.* **2020**, *8*, No. 17.
(9) Chandel, M. K.; Kwok, G.; Jackson, R. B.; et al. The potential of waste-to-energy in reducing GHG emissions. *Carbon Manage.* **2012**, *3*, 133−144.
(10) Mondino, G.; Grande, C. A.; Blom, R.; et al. Evaluation of MBTSA technology for CO2 capture from waste-to-energy plants. *Int. J. Greenhouse Gas Control* **2022**, *118*, No. 103685.
(11) Haaf, M.; Anantharaman, R.; Roussanaly, S.; et al. CO2 capture from waste-to-energy plants: Techno-economic assessment of novel integration concepts of calcium looping technology. *Resour., Conserv. Recycl.* **2020**, *162*, No. 104973.
(12) Durán, I.; Rubiera, F.; Pevida, C. Vacuum swing CO2 adsorption cycles in Waste-to-Energy plants. *Chem. Eng. J.* **2020**, *382*, No. 122841.
(13) Tsupari, E.; Arponen, T.; Hankalin, V.; et al. Feasibility comparison of bioenergy and CO2 capture and storage in a large combined heat, power and cooling system. *Energy* **2017**, *139*, 1040−1051.
(14) Gładysz, P.; Sowiżdżał, A.; Miecznik, M.; et al. Techno-Economic Assessment of a Combined Heat and Power Plant Integrated with Carbon Dioxide Removal Technology: A Case Study for Central Poland. *Energies* **2020**, *13*, No. 2841.
(15) Khorshidi, Z.; Ho, M. T.; Wiley, D. E. Techno-economic evaluation of using biomass-fired auxiliary units for supplying energy requirements of CO2 capture in coal-fired power plants. *Int. J. Greenhouse Gas Control* **2015**, *32*, 24−36.
(16) Kuramochi, T.; Faaij, A.; Ramírez, A.; et al. Prospects for cost-effective post-combustion CO2 capture from industrial CHPs. *Int. J. Greenhouse Gas Control* **2010**, *4*, 511−524.
(17) Magnanelli, E.; Mosby, J.; Becidan, M. Scenarios for carbon capture integration in a waste-to-energy plant. *Energy* **2021**, *227*, No. 120407.
(18) Luberti, M.; Oreggioni, G. D.; Ahn, H. Design of a rapid vacuum pressure swing adsorption (RVPSA) process for post-combustion CO2 capture from a biomass-fuelled CHP plant. *J. Environ. Chem. Eng.* **2017**, *5*, 3973−3982.
(19) Webley, P. A. Adsorption technology for CO2 separation and capture: a perspective. *Adsorption* **2014**, *20*, 225−231.
(20) Dhoke, C.; Zaabout, A.; Cloete, S.; et al. Demonstration of the Novel Swing Adsorption Reactor Cluster Concept in a Multistage Fluidized Bed with Heat-Transfer Surfaces for Postcombustion CO2 Capture. *Ind. Eng. Chem. Res.* **2020**, *59*, 22281−22291.
(21) Zaabout, A.; Romano, M. C.; Cloete, S.; et al. Thermodynamic assessment of the swing adsorption reactor cluster (SARC) concept for post-combustion CO2 capture. *Int. J. Greenhouse Gas Control* **2017**, *60*, 74−92.
(22) Dhoke, C.; Cloete, S.; Amini, S.; et al. Study of the Cost Reductions Achievable from the Novel SARC CO2 Capture Concept Using a Validated Reactor Model. *Ind. Eng. Chem. Res.* **2021**, *60*, 12390−12402.
(23) Zerobin, F.; Pröll, T. Concentrated Carbon Dioxide (CO2) from Diluted Sources through Continuous Temperature Swing Adsorption (TSA). *Ind. Eng. Chem. Res.* **2020**, *59*, 9207−9214.
(24) Dhoke, C.; Cloete, S.; Krishnamurthy, S.; et al. Sorbents screening for post-combustion CO2 capture via combined temperature and pressure swing adsorption. *Chem. Eng. J.* **2020**, *380*, No. 122201.
(25) Cloete, S.; Giuffrida, A.; Romano, M. C.; et al. Economic assessment of the swing adsorption reactor cluster for CO2 capture from cement production. *J. Cleaner Prod.* **2020**, *275*, No. 123024.
(26) Dhoke, C.; Zaabout, A.; Cloete, S.; et al. The swing adsorption reactor cluster (SARC) for post combustion CO2 capture: Experimental proof-of-principle. *Chem. Eng. J.* **2018**, *377*, No. 120145.
(27) Kim, K.; Seo, H.; Kim, D. J.; et al. Experimental evaluation of CO2 capture with an amine impregnated sorbent in dual circulating fluidized bed process. *Int. J. Greenhouse Gas Control* **2020**, *101*, No. 103141.
(28) Kukade, S.; Kumar, P.; Rao, P. V.; et al. Comparative study of attrition measurements of commercial FCC catalysts by ASTM fluidized bed and jet cup test methods. *Powder Technol.* **2016**, *301*, 472−477.
(29) Si, W.; Yang, B.; Yu, Q.; et al. Deactivation Kinetics of Polyethylenimine-based Adsorbents Used for the Capture of Low Concentration CO(2). *ACS Omega* **2019**, *4*, 11237−11244.
(30) Choi, W.; Min, K.; Kim, C.; et al. Epoxide-functionalization of polyethyleneimine for synthesis of stable carbon dioxide adsorbent in temperature swing adsorption. *Nat. Commun.* **2016**, *7*, No. 12640.
(31) del Pozo, C. A.; Cloete, S.; Álvaro, Á. J. Standard Economic Assessment (SEA) Tool. https://bit.ly/3IXPWC8, 2021.
(32) del Pozo, C. A.; Cloete, S.; Álvaro, Á. J. SEA Tool User Guide. https://bit.ly/3jq9Bkf, 2021.
(33) Turton, R.; Bailie, R. C.; Whiting, W. B.et al. *Analysis, Synthesis and Design of Chemical Processes: Appendix A*; Pearson Education, 2008.
(34) Woods, D. R. *Rules of Thumb in Engineering Practice*; Wiley-YCH, 2007; p 383.
(35) Feron, P. H. M.; Cousins, A.; Jiang, K.; et al. An update of the benchmark post-combustion CO2-capture technology. *Fuel* **2020**, *273*, No. 117776.

https://doi.org/10.1021/acs.energyfuels.3c00885
Energy Fuels 2023, 37, 12030−12044